PAPER

Check for updates

Monomeric M(II) (M = Fe, Co, Ni) complexes supported by bulky aryloxide ligands tethered to an arene functionality; synthesis, electrochemistry and study of the M(II)−arene interaction†

Ioannis Vagiakos, [ID] [a,b] Nikolaos Tsoureas, [ID] *[a] Tianyin Huang, [ID] [b]
Stella Christodoulou,[c] Laurent Maron, [ID] *[c] Thomas Pickl, [ID] [b] János Mink[d,e] and
Dominik P. Halter [ID] *[b,f]

The aminolysis reaction between MN''_2 ($N'' = N(SiMe_3)_2$; M = Fe, Co, Ni) and the neutral pro-ligand 6,6'-(1,4-phenylenebis(propane-2,2-diyl))bis(2,4-di-*tert*-butylphenol) (**LH₂**) affords the low coordinate, iso-morphous, monomeric bis-aryloxide complexes (**2-M**) (M = Fe, Co, Ni). Their molecular structures all feature a basal arene functionality, poised to interact with the metal centre, anchored by two sterically encumbering pendant aryloxide arms. Complexes (**2-M**) show metal–arene interactions with decreasing strength from (**2-Ni**), to (**2-Co**) and finally to (**2-Fe**). The M−arene interactions were evaluated by a combination of SC-XRD studies, supported by computational investigation and IR spectroscopic characterisation of basal−arene C−C stretches in the absence and the presence of THF in their coordination sphere. The mono-THF adducts (**2-Fe·THF**) and (**2-Co·THF**) were also synthesised, isolated and structurally characterised, showing that the M−arene interaction is disrupted upon THF coordination. Cyclic voltammetry (CV) studies of (**2-Fe**) and (**2-Co**) show reversible M^{2+}/M^+ reduction waves in non-coordinating solvent, and more complex redox chemistry upon THF coordination with (**2-Fe·THF**) and (**2-Co·THF**) in THF.

[a]Department of Chemistry, National and Kapodistrian University of Athens, Inorganic Chemistry Laboratory, Panepistimioupoli Zografou, Athens, 15772, Greece. E-mail: ntsoureas@chem.uoa.gr

[b]Chair of Inorganic and Metal-Organic Chemistry, Department of Chemistry, Catalysis Research Center (CRC), TUM School of Natural Sciences, Technical University of Munich, Lichtenbergstr. 4, 85748 Garching, Germany

[c]Université de Toulouse and CNRS, INSA, UPS, CNRS, UMR 5212, Toulouse 31077, France. E-mail: Laurent.maron@irsamc.ups-tlse.fr

[d]Institute of Materials and Environmental Chemistry, Research Center of Natural Sciences, Hungarian Academy of Sciences, Magyar Tudósok Körútja 2, Budapest H-1519, Hungary
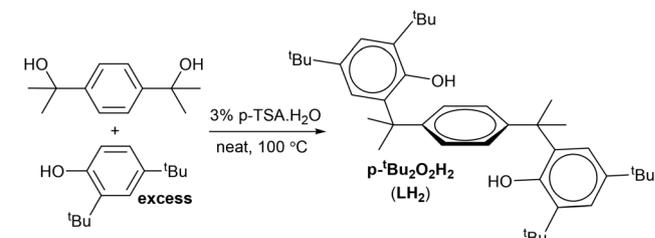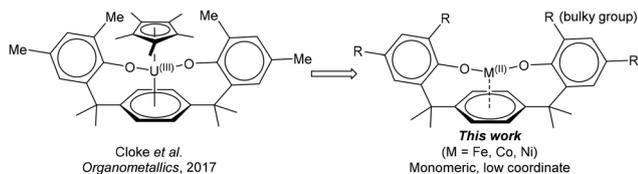
[e]Research Institute for Biomolecular and Chemical Engineering, University of Pannonia, Veszprém H-8200, Hungary

[f]Research Group Applied Electrochemistry & Catalysis (ELCAT), Faculty of Applied Engineering, Department of Biochemical and Chemical Engineering, University of Antwerp, Universiteitsplein 1, 2610 Antwerp, Belgium. E-mail: Dominik.Halter@uantwerp.be

†Electronic supplementary information (ESI) available: For compound synthesis, spectroscopic characterisation, cyclic voltammetry experiments, computational supplementary information and SC-XRD collection and refinement details. CCDC 2413653–2413658. For ESI and crystallographic data in CIF or other electronic format see DOI: https://doi.org/10.1039/d5dt00482a

Introduction

Bulky aryloxides and related alkoxides, are versatile supporting ligands that promote a variety of reactions at metal centres across the periodic table.[1,2] As ancillary ligand moieties they have been combined with a variety of other ligand functionalities (N, P, O, S and carbene donors) in a wide range of scaffolds encompassing bidentate,[3–14] pincer,[15–27] tripodal[28–31] and multidentate[32–48] architectures. In these various scaffolds, the incorporation of bulky groups (*e.g.* Ad, *[t]*Bu, aryl) in the proximity of the O^- donor atoms is an established strategy to suppress the formation of multinuclear bridged species,[49] and for aryloxides allows the isolation of homoleptic low coordinate M(II)−OAr₂ complexes (M = Mn,[50–52] Fe,[50–58] Co,[53,59] Cu[60,61]).

Expanding on this versatility, tethering two or more RO^- (R = aryl, Si(OR'), alkyl) ligands to a basal arene has proved beneficial in stabilising both d-[62–64] and f-block complexes,[65–69] with modifications of this ligand design encompassing either other anionic donors like bulky phosphinimides,[70–73] terphenyl sulfido[74] and amido ligands,[75–78] or neutral L donors such as phosphines[79–86] and NHC's.[87] In some of these examples, the basal arene anchor acts as a redox non-innocent ligand, crucial to observed reactivity.[65,79,80,82–85,88–92]

In 2017 Cloke and coworkers reported on the synthesis and reductive reactivity towards CO_2 of the U(III) complex shown in Fig. 1 (left), which is co-supported by two aryloxide ligand moieties tethered to a central arene.[93] This scaffold was selected as a potentially iso-electronic L_3X_2 (based on the CBC model)

Fig. 1 Left: A U(III) mixed sandwich complex supported by two aryloxide ligands tethered to a central arene; right: sterically encumbered monomeric low coordinate M(II) aryloxide complexes.

Scheme 1 Synthesis of neutral p-$^{t}Bu_2O_2H_2$ (LH$_2$).

'harder' flexible chelating ligand alternative to the {COT/Pn$^{(1,4-SiR3)}$}$^{2-}$ (COT = cyclooctatetraene; Pn = pentalene; R = ^{i}Pr, Me) ligands used by this group, with tuneable sterics, and with the central arene ideally situated to interact with the low valent U centre. Inspired by these advantageous attributes, we sought to expand the use of this structural motif to 3d transition metals in the formal oxidation state +2. We envisioned that modifying the flexible architecture of the scaffold to incorporate bulky R-groups in the 2,4 positions of the pendant aryloxide arms, would allow access to low coordinate 3d transition metal complexes, helped by the promotion of a metal arene interaction as a result of the organization of the coordination environment as shown on the right-hand side of Fig. 1. Furthermore, this could offer the opportunity to probe the M(II)–arene interaction (M = 3d TM) as a function of the metal centre and help establish their potential role as another redox-non innocent moiety of the ligand along the aryloxide pendant donors.[94]

In this paper we describe the synthesis and structural characterization of three such M(II) complexes (M = Fe, Co and Ni) and two of their THF adducts (Fe, Co), together with selected spectroscopic and cyclic voltammetry studies. We show that in the ligand motif of this series of complexes (Fig. 1), through bulky aryloxide ligands with CMe$_2$ bridges the arene base is held in place near the metals; albeit, with structural flexibility that allows metal–arene interactions without strictly enforcing them. DFT calculations further support the presented experimental data on metal–arene bonding interactions, to gain more detailed insight into the individual electronic structure and the extent of the respective M(II)–arene interactions.

Results and discussion

Synthesis and characterisation of pro-ligand p-$tBu_2O_2H_2$ (LH$_2$)

For our study we opted to incorporate *tert*-butyl substituents as the bulky R groups in the 2,4 positions of the aryloxide moieties of the ligand scaffold shown in Fig. 1. This modification aims to (a) prevent the formation of oxygen bridged complexes, thereby stabilizing low coordinate transition metal (TM) complexes of smaller 3d metal ions, (b) engender kinetic stability and (c) increase solubility in organic solvents with low polarity. This neutral pro-ligand p-$^{t}Bu_2O_2H_2$ (LH$_2$) can be easily accessed as a white spectroscopically and analytically pure air-stable crystalline solid in moderate yields (*ca.* 38%) *via* a one-
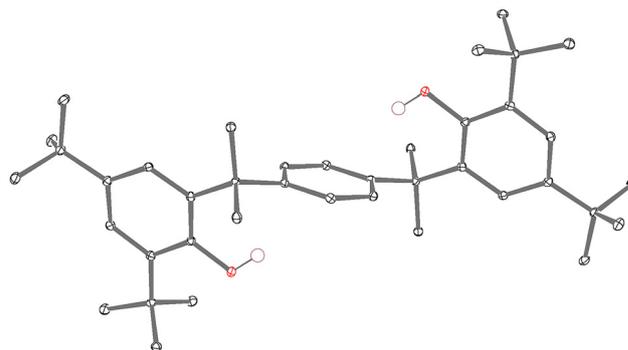

Fig. 2 ORTEP diagram of the molecular structure of the neutral pro-ligand LH$_2$, showing 50% ADP's. Hydrogen atoms, except those of the –OH groups, were omitted for clarity.

step Friedel–Crafts condensation (Scheme 1), following a slightly modified procedure described by Cloke *et al.* for their methyl substituted version.[93]

In terms of spectroscopic characterisation, LH$_2$ exhibits well interpretable ^{1}H and $^{13}C\{^1H\}$-NMR spectra ($\delta(C_6D_6)$) (Fig. S1 and 2†) with the OH protons appearing as a singlet, centred at 4.53 ppm in its ^{1}H-NMR spectrum. Furthermore, its solid-state IR spectrum displays a strong resonance at 3505 cm^{-1} (Fig. S16a & b†) characteristic of the (Ar)O–H stretching mode. Finally, the molecular structure of LH$_2$ was determined by a SC-XRD study (Fig. 2), revealing an anti-peri-planar arrangement of the pendant ArOH moieties with respect to the central arene. The average C–C bond distances of the planar central arene and aryloxide groups were found to be 1.395(1) and 1.398(1) Å, respectively. Interestingly, no inter-molecular hydrogen bonds are observed in the solid-state structure of LH$_2$.

Synthesis and characterisation of [M$^{(II)}$(p-$^{t}Bu_2O_2$)] (2-M) (M = Fe, Co, Ni) complexes

Initial attempts to prepare bis aryloxide complexes of the general formula [M$^{(II)}$(p-$^{t}Bu_2O_2$)] (2-M) (M = Fe, Co, Ni) *via* salt metathesis reactions between K$_2$(THF)$_x$L (see ESI† for synthesis and characterisation) and one molar equivalent of anhydrous MX$_2$ salts(X = Cl, Br; M = Fe, Co) in toluene produced invariably intractable mixtures.

As an alternative, the aminolysis route shown in Scheme 2, was successful for the synthesis of complexes (2-M). Indeed,
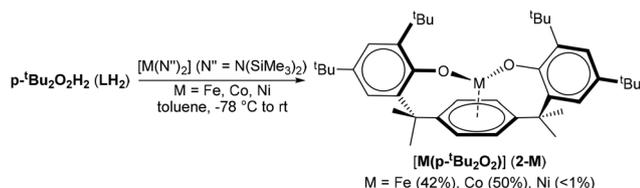
Scheme 2 General synthetic route for the preparation of complexes (**2-M**) (M = Fe, Co, Ni). In parenthesis the isolated crystalline yields of complexes (**2-M**); in the case of (**2-Ni**) only a few crystals could be isolated.

reactions of $[M(N''_2)]$ $[N'' = -N(SiMe_3)_2]$; M = Fe,[50,52,53,95] Co[59,96]] with one molar equivalent of neutral **LH$_2$** in toluene proceed very well, affording golden-yellow (**2-Fe**) and forest-green (**2-Co**) as extremely air-sensitive crystalline solids in reasonable yields of *ca.* 42 and 50% respectively. In the case of (**2-Ni**) only a small crop of brown-red crystals could be isolated, enough only for a SC-XRD study. This is the first example of $[Ni(N''_2)]$ been used to access aryloxide complexes. Unfortunately, the preparation of (**2-Ni**) proved capricious due to the thermal instability of $[Ni(N''_2)]$,[97,98] hindering its reproducible synthesis and use in follow-up reactions. Despite our best efforts, attempts to access further samples of (**2-Ni**) that could qualify for further characterization beyond SC-XRD, either *via* salt metathesis reactions in various solvents between (**2-K$_2$**) and various Ni(II) sources (NiX$_2$; X = Cl, Br, I, η^5-Cp[99]) or *via* the reaction between Ni(η^4-COD)$_2$ (COD = 1,5-cyclo-octadiene) and **LH$_2$**,[100,101] were unsuccessful. Therefore, only the structural features of (**2-Ni**) as well as results from theoretical calculations relating to it are discussed.

The identity of all three complexes (**2-M**) was unambiguously established *via* SC-XRD, which confirmed their solid-state molecular structures (Fig. 3) and our original hypothesis that the ^{t}Bu substituents indeed prevent the formation of bridged species.

As can be seen in Fig. 3, all three complexes are isomorphous with two aryloxide O$^-$ donor moieties coordinating to the metal centre in a *syn*-fashion with respect to the central arene. Assigning the base-arene centroids as a proxy for the arene as a ligand, the sum of angles around the metal centres in complexes (**2-M**) are 360° (Fe), 358.13° (Co) and 359.97° (Ni). Thus, the coordination geometry in this series of complexes can be viewed as trigonal.

The two M–O bond distances (M = Co, Ni) are the same within esd's, while in the case of (**2-Fe**) they differ slightly. In the case of (**2-Fe/Co**) these distances lie towards the lower end of the M(II)–(terminal)OAr bond-length range in the literature (Fe(II): 2.07–1.81 Å,[44,45,50,52,57,58,102–111] Co(II): 2.08–1.83 Å (ref. 11, 23, 24, 28, 51, 59, 112–121), while in the case of (**2-Ni**) the Ni–O bond distances lie in the middle of the range previously observed (2.04–1.79 Å (ref. 8, 13, 22, 27, 42, 48, 116, 122–127)) for Ni(II)-(terminal)OAr complexes. The M–O–C(*ipso*) angles of *ca.* 120° throughout the series, suggest that the M–O bond in (**2-M**) features a π-component. At the same time, the O–M–O bond angle decreases across the series from 133.76(4)° (**2-Fe**), to 122.04(7)° (**2-Co**), to the least obtuse value of 96.07(13)° for (**2-Ni**). In agreement with DFT results (*vide infra*), this can be rationalized by increasing metal–arene interactions. This is reflected by the shortening of the M–Cent distances from 2.1419(5) Å for (**2-Fe**) to 1.908(3) Å for (**2-Co**) and finally to 1.644(5) Å for (**2-Ni**). The same trend holds for the M–C$_{avg}$ bond distances, which are significantly shorter for (**2-Ni**) (2.164(2) Å) than for (**2-Co**) (2.369(1) Å) and (**2-Fe**) (2.514(4) Å).

Based on our structural data, the interaction between the M(II) metal centre and the central arene can be described as a long η^4 for (**2-Fe**) and in the case of (**2-Co**) as an η^6 interaction. The average C–C bond distances of the central arenes in (**2-Fe/Co**) are the same within esd's and indistinguishable from the one in **LH$_2$** within the 3σ criterion. In both (**2-Fe**) and (**2-Co**), an increased maximum central arene torsion angle (Table 1) is observed compared to **LH$_2$**, which we attribute to the strain imposed on this ring for the two aryloxide moieties to coordinate in the same face.

Complex (**2-Ni**) coordinates the central arene in an η^6 fashion with an Ni–centroid distance of 1.644(5) Å, which is one of the shortest observed in the literature amongst Ni(II)–(η^6-arene) complexes (Ni–Cent range: 1.635–1.731 Å (ref. 128–134)). Moreover, the planarity of the central arene is significantly perturbed as seen by the increase in the observed maximum torsion angle of 15.0(4)°, which is *ca.* three-times larger than in (**2-Fe/Co**). Simultaneously, the average C–C bond distance of the central arene is elongated to 1.411(2) Å in (**2-Ni**) (longest C–C bond: 1.427(6) Å; shortest C–C bond 1.393(6) Å) compared to 1.395(1) Å in **LH$_2$**.

Beyond SC-XRD, complexes (**2-Fe**) and (**2-Co**) were further spectroscopically and analytically characterised. Their ^{1}H-NMR spectra (δ(C$_6$D$_6$)) span the chemical shift range from −150 to
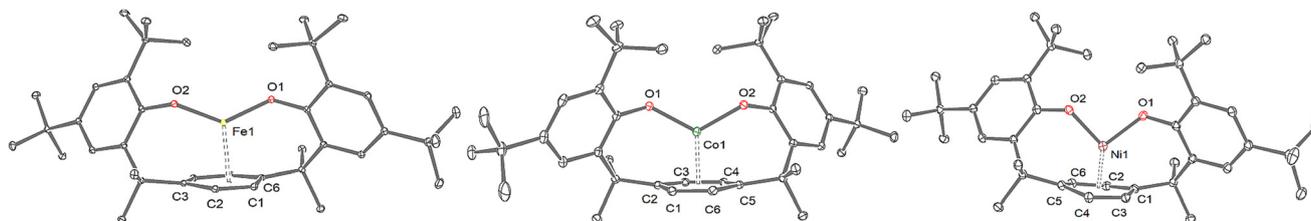

Fig. 3 ORTEP diagrams of the molecular structures of complexes (**2-M**) (from left to right M = Fe, M = Co, M = Ni) showing 50% ADP's. Hydrogen atoms and co-crystallised solvents (a molecule of C$_7$H$_8$ per asymmetric unit for (**2-Fe**) and (**2-Co**) and a molecule of C$_6$H$_{18}$ per asymmetric unit for (**2-Ni**)) were omitted for clarity.

Table 1 Selected metric parameters for complexes (2-M)

Compound	M-O (Å)	Central arene C-C (avg., Å)	Longest M-C[a] (Å)	Shortest M-C[a] (Å)	M-C$_{(arene)}$ (avg., Å)	M-Cent[c] (Å)	O1-O2 distance (Å)	O-M-O (°)	Central arene torsion angle[d] (°)	O-M-C(ipso) (°)
(2-Fe)	1.8628(7)(O1) 1.8663(7)(O2)	1.4025(4)[b]	2.5006(8) (C3)	2.4873(8) (C2)	2.514(4)	2.1419(5) (η^4)	3.4298(10)	133.76(4)	5.73(9)[e]	125.17(7) 129.57(5)
(2-Co)	1.8723(14)(O1) 1.8786(15)(O2)	1.405(1)[b]	2.4044(19) (C3)	2.346(2) (C6)	2.369(1)	1.908(3) (η^6)	3.281(2)	122.04(7)	5.4(3)	121.29(4) 124.02(12)
(2-Ni)	1.873(3) (O1) 1.864(3) (O2)	1.411(2)[b]	2.238(4) (C2)	2.093(4) (C5 & C1)	2.164(2)	1.644(5) (η^6)	2.779(5)	96.07(13)	15.0(4)	119.5(2) 120.7(2)
LH$_2$	N/A	1.395(1)[b]	N/A	N/A	N/A	N/A	7.242(3)	N/A	0.2(3)	109.6(15)[f]

[a] Refers to C atom in the basal arene. [b] esd's were calculated based on the formula $\sigma = \sqrt{\dfrac{\sum_N (\sigma_i)^2}{N}}$, where σ_i is the esd of i-th measurement and N is the number of measurements (i.e. 6 in this case). [c] Cent = basal arene centroid. [d] The largest dihedral angle between adjacent three-carbon planes in the central arene ring. [e] Modulus value. [f] Refers to the H-O-C(ipso) bond angle.

100 ppm and show 6 resonances in a 2 : 2 : 4 : 12 : 18 : 18 ratio, consistent with a C_2 symmetry in solution and in accordance with their solid-state molecular structures, which are retained in solution. The magnetic susceptibilities for (2-Fe) and (2-Co) in solution at 27 °C (Evans method) were found to be 4.20 and 3.40μ_B respectively. The latter is in good agreement for an $S = 3/2$ ground electronic state for (2-Co), albeit somewhat lower than the expected spin-only value of 3.87μ_B. Similarly, the $\mu_{eff.}$ value for (2-Fe) is borderline between a quartet and a quintet electronic ground state ($S = 2$; spin-only value 4.90μ_B), but based on theoretical calculations and the μ_{eff} of its THF adduct (see also below), we favour the latter. Power $et\ al.$ have also observed lower than expected magnetic susceptibilities in low coordinate Fe(II) and Co(II) aryl thiolate complexes in trigonal coordination geometry, due to metal–arene interactions with one of the arene wingtips of their aryl–thiolate ligand.[134] Combustion analyses were consistent with the expected molecular formulas of (2-Fe) and (2-Co) after loss of crystallization solvent (toluene) which proceeds with an observed loss of their crystallinity upon prolonged drying under vacuum.

Furthermore, IR spectroscopy (neat, solid state) was employed to (i) exclude hydrolysis leading to LH$_2$ and (ii) assess the degree of the metal–arene interactions. With respect to (i) the absence of the characteristic O–H stretch at 3500 cm^{-1} for neutral pro-ligand LH$_2$ excludes free pro-ligand impurities in samples of (2-M) (M = Fe, Co). To assess the extent of metal–arene interactions, we evaluated an IR band that corresponds to an aromatic in plane C–C ring stretch of the basal arene that is observed at 1508 cm^{-1} in pure ligand LH$_2$ (Fig. 4). Upon coordination of metal ions, we observed that this aromatic C–C stretch shifts to lower energies (1495 cm^{-1} for (2-Fe) and 1487 cm^{-1} for (2-Co)),[135] indicative
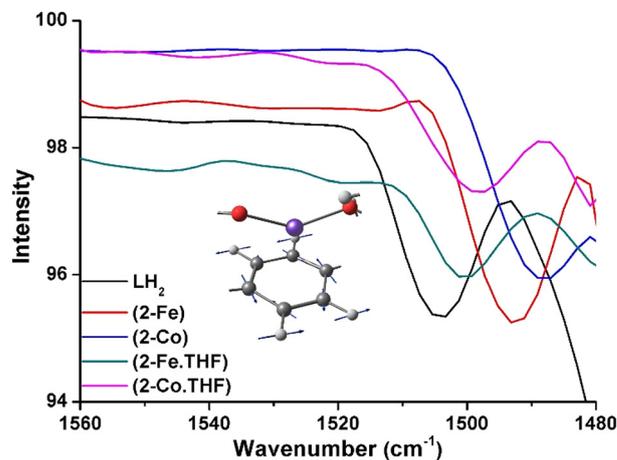

Fig. 4 Stacked IR spectra (solid state) in the region between 1560−1480 cm^{-1} for LH$_2$ (black), (2-Co) (blue), (2-Fe) (red), (2-Co·THF) (pink), (2-Fe·THF) (green). Inset: graphical representation of the corresponding C–C ring stretch mode, exemplarily shown for complex (2-Fe), for which it was calculated at 1495 cm^{-1}; image shows a truncated structure of the complex (2-Fe) with the basal arene ring at the bottom, carbon atoms in grey, H-atoms in light grey, oxygen atoms in red, and Fe in purple.

for a weakening of the C–C bond upon interaction with the metals. This suggests that the shorter crystallographic M–arene$_{centr.}$ distance for (**2-Co**) (1.908(3) Å *vs.* 2.514(4) Å in (**2-Fe**)) coincides with a stronger Co($_{II}$)–arene interaction, which DFT analysis confirmed to be a donation of metal d-electron density into arene π* acceptor orbitals (see below for details). The calculated values for these C–C vibrational modes are (1484 cm^{-1} for (**2-Co**) and 1495 cm^{-1} for (**2-Fe**)) and are in very good agreement with the experimentally observed ones, thus confirming their diagnostic value.[136] As a next step, we proceeded to assess the response of metal–arene interactions in (**2-M**) upon addition of an L-type ligand. Exemplarily, addition of THF to samples of (**2-M**) (M = Fe, Co), followed by removal of volatiles and acquisition of IR spectra of the resulting solids, shows that the C–C ring stretches of the basal arene shift back towards the value found for **LH₂** ligand, both close to *ca.* 1500 cm^{-1}. This indicated that in these two new species, presumably the THF adducts (**2-Co·THF**) and (**2-Fe·THF**), the metal arene interactions are considerably reduced, which is also in agreement with DFT calculated values of 1497 cm^{-1} and 1502 cm^{-1} for the respective THF adduct species. Therefore, we proceeded to synthesize, isolate and characterise these (**2-M·THF**) (M = Fe, Co) complexes in detail, to confirm the disruption of the metal arene interaction upon THF coordination.

Synthesis and characterisation of THF adducts (2-M·THF) (M = Fe, Co)

When (**2-Co**) and (**2-Fe**) were dissolved in d^8-THF, an immediate colour change from forest-green to brown-reddish and from golden-yellow to pale yellow respectively was observed.

In both cases, ^{1}H-NMR spectroscopy revealed the same pattern observed for the resonances of (**2-Co**) and (**2-Fe**), with some differences in their chemical shifts between the two solvents. The most substantial change was observed for the resonances attributed to the central arene protons in (**2-Fe**) that resonate at *ca* −147 ppm in C$_6$D$_6$, as they are shifted downfield to −78 ppm in d^8-THF.

The identity of these new complexes as the mono THF adducts (**2-M·THF**) was unambiguously confirmed by SC-XRD studies on crystals grown by slow cooling (−30 °C) of a THF/*n*-hexane solution for (**2-Fe·THF**), or in the case of (**2-Co·THF**) from *n*-pentane with a few drops of THF (Scheme 3 & Fig. 5).

As can be seen from Fig. 5, the coordination geometry in complexes (**2-M·THF**) can be described as distorted trigonal
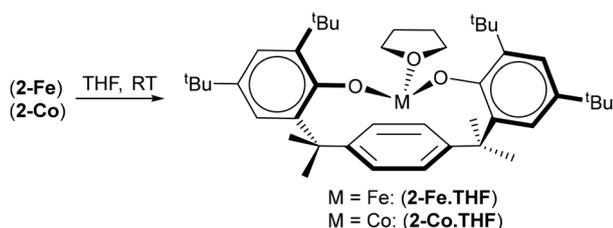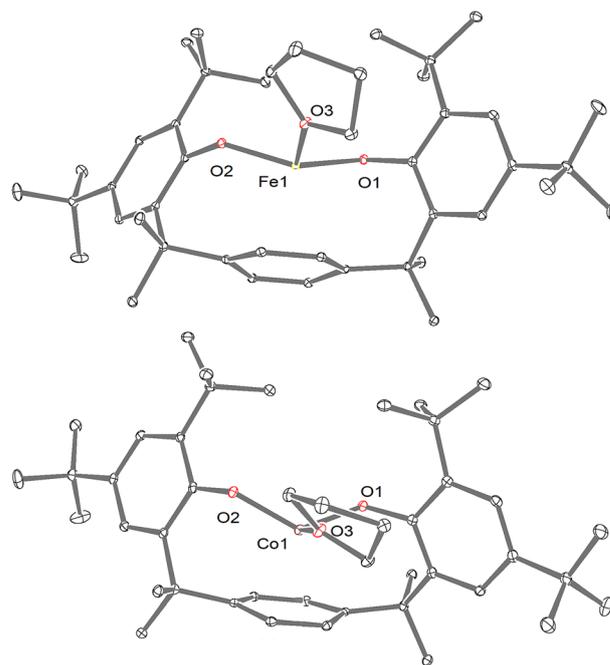

Fig. 5 ORTEP diagrams of the molecular structures of (**2-Fe·THF**)(top) and (**2-Co·THF**) (bottom) showing 50% ADP's. Hydrogen atoms and crystallisation solvent (THF in the case of (**2-Fe·THF**)) have been omitted for clarity.

(Σ°Fe = 339.48°, Σ°Co = 327.49°) with the metal centres lying below the plane of the three O donors by *ca.* 0.49 Å for (**2-Fe·THF**) and 0.63 Å for (**2-Co·THF**). The most salient difference between complexes (**2-M·THF**) and (**2-M**) (M = Fe, Co) is the disruption of the already weak M–arene interaction in the latter, upon THF coordination. Structurally this is manifested by the displacement of the metal centre by *ca.* 1.19 Å from above the central arene centroid and towards the coordinated THF in both cases (Fe–Cent(arene): 2.444(5) Å; Co–Cent(arene): 2.318(8) Å). A comparison of other metric parameters between these two types of complexes (Table 2), shows that the Fe–O(aryloxide) bond distances are elongated in (**2-Fe·THF**) compared to (**2-Fe**), whereas in the case of (**2-Co·THF**) the Co–O1 bond length increases while Co–O2 decreases slightly. In both THF adducts, a small increase is observed in the O–M–O ligand bite angle compared to complexes (**2-Fe/Co**), concomitant with an increase of the O1–O2 distance by almost 0.1 Å. The central arene average C–C bond distance is identical in all complexes and indistinguishable from the one in **LH₂**. The small increase in the maximum central arene torsion angle is again most likely associated with the bending imposed by the *syn*-coordination of the aryloxide pendant arms. Finally, it is worth pointing out that only one THF is coordinated to the metal centres, despite both complexes having been crystallised in the presence of excess THF.

The ^{1}H-NMR spectra of pale yellow (**2-Fe·THF**) and brown-red (**2-Co·THF**) in C$_6$D$_6$ exhibit resonances over a spectral width of −120 to *ca.* 75 ppm and display the same number of peaks, with their corresponding integral ratios, associated with

Scheme 3 Formation of THF adducts (**2-Fe·THF**) and (**2-Co·THF**).

Table 2 Comparison of selected metric parameters between complexes (**2-M**) and (**2-M·THF**)

Complex	M–O (Å)	O–M–O (°)	Central arene torsion angle (°)	Central arene C–C (avg., Å)
(**2-Fe**)	1.8628(7) (O1) 1.8663(7) (O2)	133.76(4)	5.73(9)	1.4025(4)
(**2-Fe·THF**)	1.8944(9) (O1) 1.8823(8) (O2)	136.16(4)	7.83(13)	1.3988(7)
(**2-Co**)	1.8723(14) (O1) 1.8786(15) (O2)	122.04(7)	5.4(3)	1.405(1)
(**2-Co·THF**)	1.8931(17) (O1) 1.8705(16) (O2)	127.57(7)	8.8(3)	1.394(1)

the coordinated L^{2-} ligand as in (**2-Fe/Co**). Furthermore, two new broad peaks integrating for 4 protons each, are also present and correspond to the coordinated THF. The spectra of (**2-M·THF**) in C_6D_6 are consistent with an average C_s structure in solution, in contrast to their C_1 static structure in the solid state. The finding confirms that THF remains coordinated in C_6D_6 solution. Their magnetic susceptibilities in solution (Evans method) at 27 °C show an increase compared to their corresponding un-solvated precursors from $4.20\mu_B$ for (**2-Fe**) and $3.40\mu_B$ for (**2-Co**) to 4.79 for (**2-Fe·THF**) and $3.70\mu_B$ for (**2-Co·THF**), respectively, and are very close to the spin-only values for an $S = 2$ ((**2-Fe·THF**)) and an $S = 3/2$ electronic ground states ((**2-Co·THF**)). Both complexes returned combustion analyses consistent with the molecular formula [(**2-M·THF**)·xTHF] (M = Fe: x = 3; M = Co: x = 1). We have also determined the THF binding constants *via* ^1H NMR titration experiments in C_6D_6, to be 63.54 (±4.91%) M^{-1} for (**2-Fe·THF**) and 216.77 (±7.15%) M^{-1} for (**2-Co·THF**). These values fit the trend found by Hevia *et al.* of smaller binding constants for [Fe(TMP)$_2$] *vs.* [Co(TMP)$_2$] (TMP = tetramethyl-piperidide) amido complexes,[137] but is opposite of the one measured for complexes [M(NDippSiMe$_3$)$_2$] (M = Fe, Co; Dipp = 2,6-^{i}Pr$_2$-C_6H_3) by Power and co-workers.[138] Attempts to fit our data to more than one coordinating THF returned values with exceedingly high errors, suggesting that the extra THF found from our elemental analyses results, is non-coordinating and most likely residual THF in the crystalline samples.

Computational investigations

As already addressed in context of IR-spectroscopic analysis above, DFT calculations (B3PW91 functional) were carried out, to gain insights into the metal–arene interaction. Initially for

(**2-Fe**) and (**2-Co**) different spin states were considered computationally. In both cases, the high spin states $S = 3/2$ for (**2-Co**) and $S = 2$ for (**2-Fe**) were found to be the ground state with the calculated metric parameters of their optimized geometries comparing well with the ones determined by SC-XRD studies, except for the Fe–Cent computed distance that was found to be longer by 0.09 Å (Table 3). In the case of (**2-Ni**) a closed-shell configuration ($S = 0$) was determined to be the ground state, which is expected for a d^8 complex, with its computed metric parameters being in good agreement with the SC-XRD determined molecular structure.

The arene–metal interaction was then analyzed using Molecular Orbital and Natural Bonding Orbital (NBO) approaches. For (**2-Ni**), the Ni–C_{arene} Wiberg Bond Indexes (WBI) are 0.2, indicating an arene–Ni interaction but with little covalency (for the sake of comparison, the Ni–O WBI are 0.4).

This is further highlighted by analyzing the HOMO−7 and HOMO−8 orbitals, which show a distinct but weak d-arene overlap (Fig. 6 – top). At the second donor acceptor level, a donation from the arene to an empty sd hybrid orbital on Ni is also found, in line with the Natural Population Analysis (NPA) pointing to a positively charged nickel (1.05) and negatively charged carbon at the arene. Applying the same analysis for (**2-Co**), the Co–C WBI indexes are lower (0.07) than in (**2-Ni**), indicating a weak covalent interaction and in line with the observed longer Co–C_{cent} distance. Nevertheless, the alpha HOMO−6 and beta HOMO−5 orbitals (Fig. 6 – bottom) show an overlap between an occupied d orbital at Co and the π^* of the arene, which is reminiscent of a δ-bonding interaction. The Canonical Molecular Orbital analysis available in NBO6 indicates that this is a metal to ligand donation, further corroborated by the NPA analysis showing a negative charge (−0.58)

Table 3 Key metric parameters derived from calculated structures of (**2-M**) and (**2-M·THF**) (M = Fe, Co)

Complex	M–O (Å)	O–M–O (°)	Central arene torsion angle (°)	Central arene C–C (avg., Å)	M–Cent (Å)	M–C average (Å)
(**2-Fe**)	1.857	140.04	5.56	1.407	2.175	2.582[a]
(**2-Co**)	1.883	126.90	5.54	1.404	1.981	2.429
(**2-Ni**)	1.856	97.15	16.44	1.413	1.679	2.192
(**2-Fe·THF**)	1.881; 1.895	141.50	7.49	1.401	2.474	1.401
(**2-Co·THF**)	1.889; 1.911	130.43	7.91	1.402	2.367	1.402

[a] Average of four shortest Fe–C(arene) bond distances.
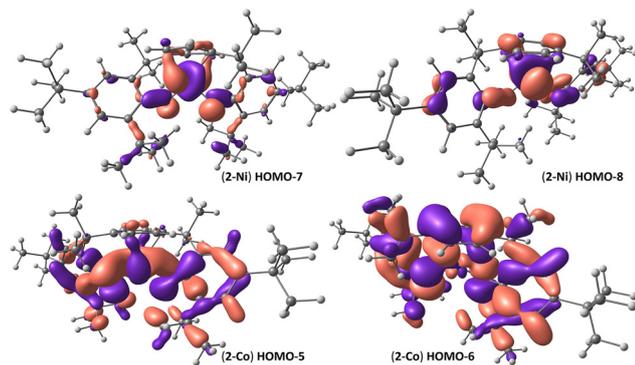
Fig. 6 Top: Calculated HOMO−7 and HOMO−8 for (**2-Ni**); bottom: calculated HOMO−5 and HOMO−6 for (**2-Co**).

Fig. 7 Top left: CV (1st scan) of (**2-Fe**) measured cathodically at 200 mV s^{-1}; top right: scan rate dependence of the process at $E_{1/2}$ = −2.13 V (*vs.* Fc/Fc$^+$) observed in the CV of (**2-Fe**); conditions: 2.7 mM of (**2-Fe**) in 3 ml 1,2-DFB with 0.1 M TBAPF$_6$; bottom left: CV (1st scan) of (**2-Co**) measured cathodically at 200 mV s^{-1}; bottom right: scan rate dependence of the process at $E_{1/2}$ = −1.67 V (*vs.* Fc/Fc$^+$) observed in the CV of (**2-Co**); conditions: 1.5 mM of (**2-Co**) in 5 ml 1,2-DFB with 0.06 M TBAPF$_6$.

at Co. This is in striking difference with (**2-Ni**) where our analysis shows a ligand to metal donation. In the case of (**2-Fe**) the Fe–C WBI indexes are the lowest of the series (0.05) and the highest occupied orbitals do not show any metal–arene interaction (pages S68–S70†). This trend is in line with the longest Fe–C$_{cent}$ distances seen experimentally and the weakest shift of the C–C IR stretch. However, it has to be noted that the overestimation of the Fe–Cent(arene) distance by almost 0.1 Å in the calculated *vs.* the SC-XRD determined structure could account for this subtle interaction not being captured by the computational model in this specific case.

Finally, the same computational analysis for (**2-Fe·THF**) and (**2-Co·THF**) found that their ground electronic states are S = 2 and S = 3/2 respectively and in both cases the M–Cent distances are lengthened to 2.367 Å for (**2-Co·THF**) and 2.474 Å for (**2-Fe·THF**). The M–C$_{arene}$ WBI indexes are almost 0 in (**2-M·THF**) complexes, concurring with the lack of any metal–arene interaction.

Cyclic voltammetry studies

With complexes (**2-M**) and (**2-M·THF**) at hand, we undertook cyclic voltammetry studies, to investigate their redox behavior.

Fig. 7 shows the CVs of (**2-Fe**) (top, left and right) and (**2-Co**) (bottom, left and right), both measured in 1,2-difluorobenzene (1,2-DFB) with [N(*n*-Bu)$_4$]PF$_6$ (TBAPF$_6$) as supporting electrolyte. 1,2-DFB was chosen as a non-coordinating polar solvent in view of the facile formation of (**2-M·THF**) and instead of DCM, which causes instantaneous decomposition of complexes (**2-M**) as seen by the formation of black precipitates.

In the case of (**2-Fe**), three processes are observed in the electrochemical window between −3.0 and 1.0 V (*vs.* Fc$^+$/Fc): one quasi reversible event at $E_{1/2}$ = 0.16 V (i_a/i_c = 1.52; ox$_1$, Fig. 7 top right), one irreversible process with an E_{pa} of −0.60 V and finally a quasi-reversible process at $E_{1/2}$ = −2.14 V (red$_1$ Fig. 7 top right and left), all of which appear in the CV of (**2-Fe**) regardless of the scan direction. We assign the redox event at +0.16 V as an oxidation event. Related iron-aryloxide complexes in the literature show ligand-based oxidation waves in this region, which were assigned to aryl-oxide oxidations.[94]
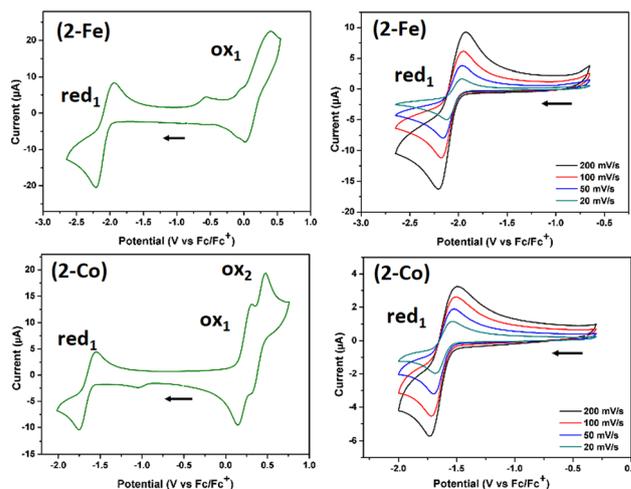
Such an assignment would also be in agreement with the calculated alpha HOMO and HOMO−1 MOs (pages S68 and S69†) of (**2-Fe**), which have mainly aryloxide character. We therefore tentatively assign the oxidation event of (**2-Fe**) to also be ligand-based but cannot fully exclude a metal-centered process within the scope of this study. CV data of the di-potassium salt (**2-K$_2$**) was measured for comparison to the ones obtained for complexes (**2-M**) (ESI, Fig. S34†). **2-K$_2$** shows one oxidation wave at −0.86 V as the only redox event. While this is in agreement with our discussion that the ligand in complexes (**2-M**) can likely also be oxidized, we note that the general differences in metal–ligand bonding situation between a potassium cation and the transition metal centres render their redox properties very different. The quasi-reversible process at $E_{1/2}$ = −2.14 V we attribute to a reduction event. The scan rate dependence of this process was studied and is shown in the top right CV of Fig. 7. Even at very slow scan rates of 20 mV s^{-1} the reduction event remains reversible to a high degree, suggesting a considerable stability of this reduced form. One plausible assignment of this reduction event arises from considering the calculated alpha and beta LUMOs of (**2-Fe**); the former are composed primarily of the pi manifold of the basal arene (page S69†) while the latter feature a delta interaction between the metal centre and the arene (page S73†). It is therefore possible that the reduction results in an intermediate valent species with partially reduced metal and partially reduced basal arene ligand character,[65,68,88,89] especially at these negative potentials. A detailed investigation of the electronic situation requires follow-up work that will be performed in the future. The irreversible process at E_{pa} = −0.61 V is most likely due to minor sample decomposition during the

measurement, which does not seem to interfere with the data interpretation.

The CV of (**2-Co**) displays three major processes (Fig. 7, bottom left). The two quasi-reversible processes with $E_{1/2}$ values 0.23 V and 0.40 V (ox$_1$ and ox$_2$ respectively in Fig. 7 bottom left) are tentatively assigned, to the same aryloxide based oxidation observed for (**2-Fe**), and the oxidation of the Co(III)/Co(II) redox couple. Considering that Co is more easily reduced than Fe, supports the hypothesis that the correlated Fe(III)/Fe(II) couple lies at slightly higher potentials and could not be observed within the accessible electrochemical solvent window under the applied conditions. The quasi-reversible reduction process at $E_{1/2} = -1.67$ V (*vs.* Fc/Fc$^+$; red$_1$ in Fig. 7 bottom left & right) is, as for the reduction in (**2-Fe**) also remarkably reversible at slow scan rates of 20 mV s^{-1}. The calculated LUMOs of complex (**2-Co**) show likewise contributions of metal d-orbitals (beta) and basal arene pi orbitals (alpha), however, in contrast to the beta LUMOs of (**2-Fe**), with less pronounced covalency. It is therefore possible that the reduction event at -1.67 V is due to the Co(II)/Co(I) redox couple.

While such species with potential for intermittent valency and dynamic rearrangement of electron density between ligand and metal centre can underpin reactivity,[88,139–141] a detailed further analysis of such behaviour remained beyond the scope of this work.

Initial attempts to isolate these seemingly chemically accessible reduced species by reacting complexes (**2-M**) (M = Fe, Co) with KC$_8$ and in the case of (**2-Co**) with CoCp$^R_2$ (R = H, Me$_5$), either in *n*-hexane or toluene, have been unsuccessful. In the first case the immediate formation of K$_2$L is observed, while in the latter case intractable reaction mixtures are produced.

Dissolving complexes (**2-Fe**) and (**2-Co**) to form (**2-M·THF**) (M = Fe, Co), resulted in significant changes to their redox behaviour, as observed by their CV's (Fig. 8 and Fig. S32 and S33†). For instance, in the CV of (**2-Fe·THF**) (Fig. 8) the reduction process has become more irreversible with a reduced anodic current response ($|i_{pa}/i_{pc}| = 0.31$), which diminishes

further with slower scan rates (Fig. S32b in ESI†) and becomes almost fully irreversible at 20 mV s^{-1} unlike for its parent THF free complex (**2-Fe**). The other major quasi reversible observed process has an $E_{1/2}$ of 0.14 V *vs.* Fc/Fc$^+$, which is again assigned to an aryloxide oxidation at the ligand. These changes in the electrochemical behavior are even more extreme in the case of (**2-Co·THF**) where the CV shows that all processes have become completely irreversible (Fig. S33 in the ESI†) and bare very little resemblence to its precursor (**2-Co**).

Conclusions

Low coordinate monomeric complexes of Fe(II), Co(II) and Ni(II) supported by a ligand with two sterically encumbering aryloxide pendant arms, connected to an arene functionality were synthesised, isolated and in the case of Fe and Co fully characterised (complexes (**2-M**)). Their molecular structures, supported by computational investigations, show an increasing degree of interaction between the metal centre M and the anchoring arene traversing the series from (**2-Fe**) with the weakest interaction, to (**2-Ni**) that shows the strongest arene bonding interaction. In the case of (**2-Fe**) and (**2-Co**), their mono-THF adducts (**2-Fe·THF**) and (**2-Co·THF**) were also synthesised, isolated and structurally characterised, showing that THF coordination disrupts any M–arene interaction. Cyclic voltammetry (CV) studies of (**2-Fe**) and (**2-Co**) point to a rich electrochemical behaviour, likely involving ligand participation in the redox events, and suggest that the reduced complexes [(**2-Fe**)]$^-$ and [(**2-Co**)]$^-$ might eventually be chemically accessible. CV studies of (**2-Fe·THF**) and (**2-Co·THF**) show that THF coordination has a significant impact in their electrochemical responses, especially in the case of (**2-Co·THF**). We are currently investigating alternative routes to a more robust preparation for (**2-Ni**) as well as isolating well-defined compounds from the reduction of (**2-Fe**) and (**2-Co**) to study their properties and electronic structures.

Author contributions

N.T. conceived the project, performed initial experiments, collected-solved-modelled-refined SC-XRD data, I.V. performed the synthesis, characterisation, IR measurements and cyclic voltammetry investigations for all compounds, T.P. supported SC-XRD analysis, collected-solved-modelled-refined SC-XRD data, D.P.H. guided CV and IR analysis, T.H. contributed NMR and CV data, D.P.H and J.M. conceived IR investigations to assess arene bonding, L.M. and S.C. performed computations, J.M. helped with the analysis of IR spectra. All authors contributed to the writing of this manuscript.

Fig. 8 CV (1st scan) of (**2-Fe·THF**) measured cathodically at 200 mV s^{-1}; conditions: 2.67 mM of (**2-Fe·THF**) in 3 ml THF with 0.17 M TBAPF$_6$.

Data availability

The data supporting this article have been included as part of the ESI.† Therein are detailed the compound synthesis, spec-

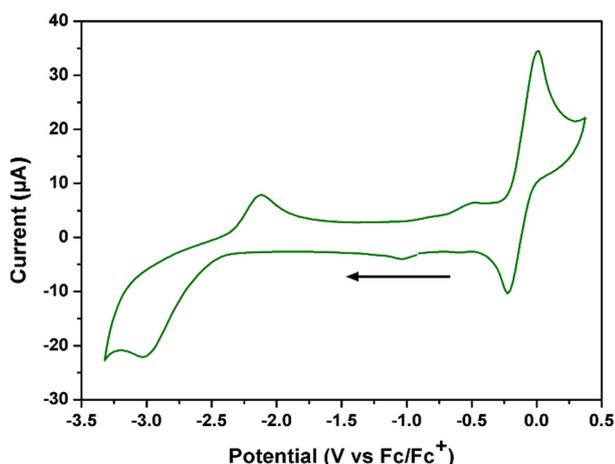troscopic characterisation (NMR, IR, UV-Vis, elemental analysis), cyclic voltammetry experiments, computational ESI† and SC-XRD collection and refinement details. With respect to crystallographic data, .cif files of reported compounds have been deposited to the CCDC with the following reference numbers: 2413653 (**LH₂**), 2413654 (**2-Fe**), 2413658 (**2-Co**), 2413655 (**2-Ni**), 2413656 (**2-Fe·THF**) and 2413657 (**2-Co·THF**).† As part of our submission, we include in our submission the Checkcif files in .pdf format. Also included as separate animated .gif files the calculated in-plane aromatic C–C basal arene stretches. All this ESI† and data are freely available.

Conflicts of interest

There are no conflicts to declare.

Acknowledgements

References

1 P. T. Wolczanski, *Polyhedron*, 1995, **14**, 3335–3362.
2 D. C. Bradley, R. C. Mehtora, I. P. Rothwell and A. Singh, *Alkoxo and aryloxo derivatives of metals*, Academic Press, 2nd edn, 2001.
3 W. Stroek, M. Keilwerth, D. M. Pividori, K. Meyer and M. Albrecht, *J. Am. Chem. Soc.*, 2021, **143**, 20157–20165.
4 L. A. Hudson, W. Stroek and M. Albrecht, *Dalton Trans.*, 2024, **53**, 14795–14800.
5 P. L. Arnold, R. W. F. Kerr, C. Weetman, S. R. Docherty, J. Rieb, F. L. Cruickshank, K. Wang, C. Jandl, M. W. McMullon, A. Pöthig, F. E. Kühn and A. D. Smith, *Chem. Sci.*, 2018, **9**, 8035–8045.
6 E. M. Matson, S. M. Franke, N. H. Anderson, T. D. Cook, P. E. Fanwick and S. C. Bart, *Organometallics*, 2014, **33**, 1964–1971.

7 Y. Konishi, W. J. Tao, H. Yasuda, S. Ito, Y. Oishi, H. Ohtaki, A. Tanna, T. Tayano and K. Nozaki, *ACS Macro Lett.*, 2018, **7**, 213–217.
8 R. Kunert, C. Philouze, O. Jarjayes, T. Storr and F. Thomas, *Organometallics*, 2023, **42**, 1550–1560.
9 Y. H. Chen, S. J. Chen, J. Q. Li, Z. Wu, G. H. Lee, Y. H. Liu, W. T. Cheng, C. Y. Yeh and C. H. Peng, *J. Polym. Sci.*, 2020, **58**, 101–113.
10 M. Z. Chen, H. M. Sun, W. F. Li, Z. G. Wang, Q. Shen and Y. Zhang, *J. Organomet. Chem.*, 2006, **691**, 2489–2494.
11 A. Mrutu, A. C. Lane, J. M. Drewett, S. D. Yourstone, C. L. Barnes, C. M. Halsey, J. W. Cooley and J. R. Walensky, *Polyhedron*, 2013, **54**, 300–308.
12 S. Xiong, H. A. Spinney, B. C. Bailey, B. S. Henderson, A. A. Tekpor, M. R. Espinosa, P. Saha and T. Agapie, *ACS Catal.*, 2024, **14**, 5260–5268.
13 S. Bertini, M. Rahaman, A. Dutta, P. Schollhammer, A. V. Rudnev, F. Gloaguen, P. Broekmann and M. Albrecht, *Green Chem.*, 2021, **23**, 3365–3373.
14 A. E. Kynman, Ab K. Luca Elghanayan, A. N. Desnoyer, Y. Yang, A. Di Giuseppe, T. Don Tilley, L. Maron and P. L. Arnold, *Chem. Sci.*, 2022, **13**, 14090–14100.
15 L. Gravogl, F. W. Heinemann, D. Munz and K. Meyer, *Inorg. Chem.*, 2020, **59**, 5632–5645.
16 A. Cadranel, L. Gravogl, D. Munz and K. Meyer, *Chem. – Eur. J.*, 2022, **28**, e202200269.
17 L. Gravogl, D. Kass, O. Pyschny, F. W. Heinemann, M. Haumann, S. Katz, P. Hildebrandt, H. Dau, A. Swain, R. García-Serres, K. Ray, D. Munz and K. Meyer, *J. Am. Chem. Soc.*, 2024, **146**, 28757–28769.
18 L. N. Saunders, M. E. Pratt, S. E. Hann, L. N. Dawe, A. Decken, F. M. Kerton and C. M. Kozak, *Polyhedron*, 2012, **46**, 53–65.
19 D. L. J. Broere, N. P. Van Leest, B. De Bruin, M. A. Siegler and J. I. Van Der Vlugt, *Inorg. Chem.*, 2016, **55**, 8603–8611.
20 D. Fujita, H. Sugimoto, Y. Morimoto and S. Itoh, *Inorg. Chem.*, 2018, **57**, 9738–9747.
21 J. Jacquet, K. Cheaib, Y. Ren, H. Vezin, M. Orio, S. Blanchard, L. Fensterbank and M. Desage-El Murr, *Chem. – Eur. J.*, 2017, **23**, 15030–15034.
22 C. Gandara, C. Philouze, O. Jarjayes and F. Thomas, *Inorg. Chim. Acta*, 2018, **482**, 561–566.
23 C. F. Harris, M. B. Bayless, N. P. Van Leest, Q. J. Bruch, B. N. Livesay, J. Bacsa, K. I. Hardcastle, M. P. Shores, B. De Bruin and J. D. Soper, *Inorg. Chem.*, 2017, **56**, 12421–12435.
24 E. P. Ivakhnenko, A. G. Starikov, V. I. Minkin, K. A. Lyssenko, M. Y. Antipin, V. I. Simakov, M. S. Korobov, G. S. Borodkin and P. A. Knyazev, *Inorg. Chem.*, 2011, **50**, 7022–7032.
25 W. Phonsri, D. S. Macedo, K. R. Vignesh, G. Rajaraman, C. G. Davies, G. N. L. Jameson, B. Moubaraki, J. S. Ward, P. E. Kruger, G. Chastanet and K. S. Murray, *Chem. – Eur. J.*, 2017, **23**, 7052–7065.
26 R. K. Gwinn, M. Williams, T. P. Latendresse, C. Slebodnick, D. Troya, T. Tarannum and D. A. Thornton, *Inorg. Chem.*, 2024, **63**, 7692–7704.

27 B. Wittwer, D. Leitner, F. R. Neururer, R. Schoch, M. Seidl, J. Pecak, M. Podewitz and S. Hohloch, *Polyhedron*, 2024, **250**, 116786.

28 M. Käß, J. Hohenberger, M. Adelhardt, E. M. Zolnhofer, S. Mossin, F. W. Heinemann, J. Sutter and K. Meyer, *Inorg. Chem.*, 2014, **53**, 2460–2470.

29 M. Adelhardt, M. J. Chalkley, F. W. Heinemann, J. Sutter, A. Scheurer and K. Meyer, *Inorg. Chem.*, 2014, **53**, 2763–2765.

30 K. W. Chou, W. J. Su, H. F. Huang, X. R. Zou, Y. N. Chang, P. Y. Lee and L. C. Liang, *Polyhedron*, 2017, **125**, 164–172.

31 L. C. Liang, Y. N. Chang, H. Y. Shih, S. T. Lin and H. M. Lee, *Eur. J. Inorg. Chem.*, 2011, 4077–4082.

32 K. S. Min, T. Weyhermüller, E. Bothe and K. Wieghardt, *Inorg. Chem.*, 2004, **43**, 2922–2931.

33 J. Bendix, K. Meyer, T. Weyhermu, E. Bill, N. Metzler-Nolte and K. Wieghardt, *Inorg. Chem.*, 1998, **37**, 1767–1775.

34 D. T. Rosa and D. Coucouvanis, *Inorg. Chem.*, 1998, **37**, 2328–2329.

35 H. Ma, T. P. Spaniol and J. Okuda, *Angew. Chem., Int. Ed.*, 2006, **45**, 7818–7821.

36 K. Beckerle, A. Sauer, T. P. Spaniol and J. Okuda, *Polyhedron*, 2016, **116**, 105–110.

37 R. Metzinger and C. Limberg, *Z. Anorg. Allg. Chem.*, 2012, **638**, 2225–2234.

38 J. Devonport, N. Bodnár, A. McGown, M. Bukar Maina, L. C. Serpell, C. Kállay, J. Spencer and G. E. Kostakis, *Inorg. Chem.*, 2021, **60**, 15310–15320.

39 S. I. Sampani, V. Zdorichenko, M. Danopoulou, M. C. Leech, K. Lam, A. Abdul-Sada, B. Cox, G. J. Tizzard, S. J. Coles, A. Tsipis and G. E. Kostakis, *Dalton Trans.*, 2020, **49**, 289–299.

40 J. Devonport, L. Sully, A. K. Boudalis, S. Hassell-Hart, M. C. Leech, K. Lam, A. Abdul-Sada, G. J. Tizzard, S. J. Coles, J. Spencer, A. Vargas and G. E. Kostakis, *JACS Au*, 2021, **1**, 1937–1948.

41 A. J. Macnair, C. R. P. Millet, G. S. Nichol, A. Ironmonger and S. P. Thomas, *ACS Catal.*, 2016, **6**, 7217–7221.

42 R. Kunert, C. Philouze, O. Jarjayes and F. Thomas, *Inorg. Chem.*, 2019, **58**, 8030–8044.

43 J. J. Wu, M. L. Cao and B. H. Ye, *Chem. Commun.*, 2010, **46**, 3687–3689.

44 H. Schroeder, B. R. M. Lake, S. Demeshko, M. P. Shaver and M. Buback, *Macromolecules*, 2015, **48**, 4329–4338.

45 G. Dyson, J. C. Frison, S. Simonovic, A. C. Whitwood and R. E. Douthwaite, *Organometallics*, 2008, **27**, 281–288.

46 H. Kawaguchi and T. Matsuo, *J. Organomet. Chem.*, 2004, **689**, 4228–4243.

47 S. Celen, E. Gungor, H. Kara and A. D. Azaz, *J. Coord. Chem.*, 2013, **66**, 3170–3181.

48 T. P. A. Cao, G. Nocton, L. Ricard, X. F. Le Goff and A. Auffrant, *Angew. Chem., Int. Ed.*, 2014, **53**, 1368–1372.

49 P. P. Power, *Chem. Rev.*, 2012, **112**, 3482–3507.

50 H. Chen, P. P. Power and S. C. Shoner, *Inorg. Chem.*, 1991, **30**, 2884–2888.

51 C. P. McLoughlin, J. C. Fettinger and P. P. Power, *Inorg. Chem.*, 2023, **62**, 10131–10140.

52 R. A. Bartlett, J. J. Ellison, P. P. Power and S. C. Shoner, *Inorg. Chem.*, 1991, **30**, 2888–2894.

53 C. R. Stennett, J. C. Fettinger and P. P. Power, *Inorg. Chem.*, 2021, **60**, 6712–6720.

54 M. B. Chambers, S. Groysman, D. Villagrán and D. G. Nocera, *Inorg. Chem.*, 2013, **52**, 3159–3169.

55 T. J. Boyle, M. L. Neville, C. A. Apblett, S. M. Hoppe and M. Gembicky, *Polyhedron*, 2013, **65**, 89–97.

56 T. Hatanaka, R. Miyake, Y. Ishida and H. Kawaguchi, *J. Organomet. Chem.*, 2011, **696**, 4046–4050.

57 D. S. Belov, L. Mathivathanan, M. J. Beazley, W. B. Martin and K. V. Bukhryakov, *Angew. Chem., Int. Ed.*, 2021, **60**, 2934–2938.

58 C. Ni and P. P. Power, *Chem. Commun.*, 2009, 5543–5545.

59 A. M. Bryan, G. J. Long, F. Grandjean and P. P. Power, *Inorg. Chem.*, 2014, **53**, 2692–2698.

60 C. Lopes, M. Håkansson and S. Jagner, *Inorg. Chem.*, 1997, **36**, 3232–3236.

61 P. Fiaschi, C. Floriani, M. Pasquali, A. Chiesi-Villa and C. Guastinib, *J. Chem. Soc., Chem. Commun.*, 1984, 888–890.

62 J. Hillenbrand, M. Leutzsch, E. Yiannakas, C. P. Gordon, C. Wille, N. Nöthling, C. Copéret and A. Fürstner, *J. Am. Chem. Soc.*, 2020, **142**, 11279–11294.

63 R. R. Thompson, M. E. Rotella, P. Du, X. Zhou, F. R. Fronczek, R. Kumar, O. Gutierrez and S. Lee, *Organometallics*, 2019, 4054–4059.

64 S. S. Kurup, D. Wannipurage, R. L. Lord and S. Groysman, *Chem. Commun.*, 2019, **55**, 10780–10783.

65 M. E. Fieser, C. T. Palumbo, H. S. La Pierre, D. P. Halter, V. K. Voora, J. W. Ziller, F. Furche, K. Meyer and W. J. Evans, *Chem. Sci.*, 2017, **8**, 7424–7433.

66 C. T. Palumbo, D. P. Halter, V. K. Voora, G. P. Chen, A. K. Chan, M. E. Fieser, J. W. Ziller, W. Hieringer, F. Furche, K. Meyer and W. J. Evans, *Inorg. Chem.*, 2018, **57**, 2823–2833.

67 H. S. Lapierre, A. Scheurer, F. W. Heinemann, W. Hieringer and K. Meyer, *Angew. Chem., Int. Ed.*, 2014, **53**, 7158–7162.

68 F. C. Hsueh, T. Rajeshkumar, L. Maron, R. Scopelliti, A. Sienkiewicz and M. Mazzanti, *Chem. Sci.*, 2023, **14**, 6011–6021.

69 M. Tricoire, F. C. Hsueh, M. Keener, T. Rajeshkumar, R. Scopelliti, I. Zivkovic, L. Maron and M. Mazzanti, *Chem. Sci.*, 2024, **15**, 6874–6883.

70 P. Rathke and J. Rittle, *Angew. Chem., Int. Ed.*, 2023, **62**, e202310482.

71 C. C. Winslow, P. Rathke and J. Rittle, *Inorg. Chem.*, 2023, **62**, 17697–17704.

72 H. B. Lee, N. Ciolkowski, M. Field, D. A. Marchiori, R. D. Britt, M. T. Green and J. Rittle, *J. Am. Chem. Soc.*, 2025, **147**, 770–779.

73 C. Winslow, H. B. Lee, M. J. Field, S. J. Teat and J. Rittle, *J. Am. Chem. Soc.*, 2021, **143**, 13686–13693.

74 I. Ćorić, B. Q. Mercado, E. Bill, D. J. Vinyard and P. L. Holland, *Nature*, 2015, **526**, 96–99.

75 D. T. Nguyen, C. Helling, M. J. Evans and C. Jones, *Inorg. Chem.*, 2024, **63**, 5718–5726.

76 J. Murillo, C. A. P. Goodwin, L. Stevens, S. Fortier, A. J. Gaunt and B. L. Scott, *Chem. Sci.*, 2023, **14**, 7438–7446.

77 C. Deng, J. Liang, R. Sun, Y. Wang, P. X. Fu, B. W. Wang, S. Gao and W. Huang, *Nat. Commun.*, 2023, **14**, 4657.

78 M. Yadav, A. Metta-Magaña and S. Fortier, *Chem. Sci.*, 2020, **11**, 2381–2387.

79 J. A. Buss and T. Agapie, *J. Am. Chem. Soc.*, 2016, **138**, 16466–16477.

80 S. Lin, M. W. Day and T. Agapie, *J. Am. Chem. Soc.*, 2011, **133**, 3828–3831.

81 C. H. Low, J. A. Buss and T. Agapie, *Inorg. Chem.*, 2022, **61**, 7710–7714.

82 J. A. Buss, P. H. Oyala and T. Agapie, *Angew. Chem.*, 2017, **129**, 14694–14698.

83 S. Suseno, K. T. Horak, M. W. Day and T. Agapie, *Organometallics*, 2013, **32**, 6883–6886.

84 K. T. Horak, A. Velian, M. W. Day and T. Agapie, *Chem. Commun.*, 2014, **50**, 4427–4429.

85 G. A. Bailey, J. A. Buss, P. H. Oyala and T. Agapie, *J. Am. Chem. Soc.*, 2021, **143**, 13091–13102.

86 J. A. Buss, G. A. Edouard, C. Cheng, J. Shi and T. Agapie, *J. Am. Chem. Soc.*, 2014, **136**, 11272–11275.

87 E. Y. Tsui and T. Agapie, *Polyhedron*, 2014, **84**, 103–110.

88 F. C. Hsueh, D. Chen, T. Rajeshkumar, R. Scopelliti, L. Maron and M. Mazzanti, *Angew. Chem., Int. Ed.*, 2024, **63**, DOI: **10.1002/anie.202317346.**

89 M. Tricoire, W. Sroka, T. Rajeshkumar, R. Scopelliti, A. Sienkiewicz, L. Maron and M. Mazzanti, *J. Am. Chem. Soc.*, 2025, **147**, 1162–1171.

90 H. S. Lapierre, H. Kameo, D. P. Halter, F. W. Heinemann and K. Meyer, *Angew. Chem., Int. Ed.*, 2014, **53**, 7154–7157.

91 D. P. Halter, C. T. Palumbo, J. W. Ziller, M. Gembicky, A. L. Rheingold, W. J. Evans and K. Meyer, *J. Am. Chem. Soc.*, 2018, **140**, 2587–2594.

92 C. T. Palumbo, D. P. Halter, V. K. Voora, G. P. Chen, J. W. Ziller, M. Gembicky, A. L. Rheingold, F. Furche, K. Meyer and W. J. Evans, *Inorg. Chem.*, 2018, **57**, 12876–12884.

93 C. J. Inman, A. S. P. Frey, A. F. R. Kilpatrick, F. G. N. Cloke and S. M. Roe, *Organometallics*, 2017, **36**, 4539–4545.

94 S. Kimura, E. Bill, E. Bothe, T. Weyhermüller and K. Wieghardt, *J. Am. Chem. Soc.*, 2001, **123**, 6025–6039.

95 D. L. J. Broere, I. Ćorić, A. Brosnahan and P. L. Holland, *Inorg. Chem.*, 2017, **56**, 3140–3143.

96 A. M. Bryan, G. J. Long, F. Grandjean and P. P. Power, *Inorg. Chem.*, 2013, **52**, 12152–12160.

97 M. Faust, A. M. Bryan, A. Mansikkamäki, P. Vasko, M. M. Olmstead, H. M. Tuononen, F. Grandjean, G. J. Long and P. P. Power, *Angew. Chem.*, 2015, **127**, 13106–13109.

98 A. M. Borys and E. Hevia, *Organometallics*, 2021, **40**, 442–447.

99 B. N. Zheng, M. O. Miranda, A. G. DiPasquale, J. A. Golen, A. L. Rheingold and L. H. Doerrer, *Inorg. Chem.*, 2009, **48**, 4274–4276.

100 A. Bismuto, P. Müller, P. Finkelstein, N. Trapp, G. Jeschke and B. Morandi, *J. Am. Chem. Soc.*, 2021, **143**, 10642–10648.

101 A. Schott, H. Schott, G. Wilke, J. Brandt, H. Hoberg and E. G. Hoffmann, *Justus Liebigs Ann. Chem.*, 1973, 508–530.

102 M. D. Walter and P. S. White, *Inorg. Chem.*, 2012, **51**, 11860–11872.

103 A. Kayal and S. C. Lee, *Inorg. Chem.*, 2002, **41**, 321–330.

104 D. Boinnard, A. Bousseksou, A. Dworkin, J.-M. Savariault and F. Varret, *Inorg. Chem.*, 1994, **33**, 271–281.

105 E. F. Chard, L. N. Dawe and C. M. Kozak, *J. Organomet. Chem.*, 2013, **737**, 32–39.

106 J. Houghton, S. Simonovic, A. C. Whitwood, R. E. Douthwaite, S. A. Carabineiro, J. C. Yuan, M. M. Marques and P. T. Gomes, *J. Organomet. Chem.*, 2008, **693**, 717–724.

107 J. M. Becker, J. Barker, G. J. Clarkson, R. Van Gorkum, G. K. Johal, R. I. Walton and P. Scott, *Dalton Trans.*, 2010, **39**, 2309–2326.

108 H. Schneider, D. Schmidt, A. Eichhöfer, M. Radius, F. Weigend and U. Radius, *Eur. J. Inorg. Chem.*, 2017, **2017**, 2600–2616.

109 J. Heinicke, A. Dal, H.-F. Klein, O. Hetche, U. Flörke and H.-J. Haupt, *Z. Naturforsch.*, 1999, **54**, 1235–1243.

110 J. Heinicke, M. He, A. Dal, H. F. Klein, O. Hetche, W. Keim, U. Flörke and H. J. Haupt, *Eur. J. Inorg. Chem.*, 2000, 431–440.

111 B. S. Hammes and C. J. Carrano, *Inorg. Chem.*, 1999, **38**, 3562–3568.

112 S. M. Shepard and P. L. Diaconescu, *Organometallics*, 2016, **35**, 2446–2453.

113 O. Iasco, G. Novitchi, E. Jeanneau, J. B. Tommasino, N. Roques and D. Luneau, *Inorg. Chem.*, 2012, **51**, 2588–2596.

114 L. Benisvy, E. Bill, A. J. Blake, D. Collison, E. S. Davies, C. D. Garner, C. I. Guindy, E. J. L. McInnes, G. McArdle, J. McMaster, C. Wilson and J. Wolowska, *Dalton Trans.*, 2004, 3647–3653.

115 X. Hong, M. Mellah, F. Bordier, R. Guillot and E. Schulz, *ChemCatChem*, 2012, **4**, 1115–1121.

116 H. Arora, C. Philouze, O. Jarjayes and F. Thomas, *Dalton Trans.*, 2010, **39**, 10088–10098.

117 T. Feng, D. Bu and H. Lei, *Polyhedron*, 2018, **148**, 109–117.

118 X. He, Y. Wang, D. Yuan, H. You and Y. Yao, *Inorg. Chem.*, 2021, **60**, 11521–11529.

119 M. Mijanuddin, D. Maity, M. Ali, M. G. B. Drew and P. C. Mondal, *Transition Met. Chem.*, 2007, **32**, 985–990.

120 C. Yuan, X. Xu, Y. Zhang and S. Ji, *Chin. J. Chem.*, 2012, **30**, 1474–1478.

121 T. C. Higgs, K. Spartalian, C. J. O'connor, B. F. Matzanke and C. J. Carrano, *Inorg. Chem.*, 1998, **37**, 2263–2272.

122 K. Herasymchuk, J. J. Miller, G. A. Macneil, A. S. Sergeenko, D. McKearney, S. Goeb, M. Sallé, D. B. Leznoff and T. Storr, *Chem. Commun.*, 2019, **55**, 6082–6085.

123 J. A. Hlina, J. R. Pankhurst, N. Kaltsoyannis and P. L. Arnold, *J. Am. Chem. Soc.*, 2016, **138**, 3333–3345.

124 A. Singh, A. Maji, A. Mohanty and K. Ghosh, *J. Organomet. Chem.*, 2021, **934**, 121631.

125 C. Y. Tsai, M. C. Huang, M. L. Lin, Y. C. Su and C. C. Lin, *Inorg. Chem.*, 2022, **61**, 19870–19881.

126 M. M. Shoshani and T. Agapie, *Chem. Commun.*, 2020, **56**, 11279–11282.

127 D. Yang, J. Dong and B. Wang, *Dalton Trans.*, 2018, **47**, 180–189.

128 A. R. O'Connor, P. S. White and M. Brookhart, *Organometallics*, 2010, **29**, 5382–5389.

129 F. Koch, A. Berkefeld, B. Speiser and H. Schubert, *Chem. – Eur. J.*, 2017, **23**, 16681–16690.

130 J. L. Priego, L. H. Doerrer, L. H. Rees and M. L. H. Green, *Chem. Commun.*, 2000, 779–780.

131 R. J. Witzke and T. D. Tilley, *Chem. Commun.*, 2019, **55**, 6559–6562.

132 J. Cámpora, M. Del Mar Conejo, M. L. Reyes, K. Mereiter and E. Passaglia, *Chem. Commun.*, 2003, 78–79.

133 M. Schmitt, M. Mayländer, T. Heizmann, S. Richert, C. Bülow, K. Hirsch, V. Zamudio-Bayer, J. T. Lau and I. Krossing, *Angew. Chem., Int. Ed.*, 2022, **61**, e202211555.

134 J. Pratt, A. M. Bryan, M. Faust, J. N. Boynton, P. Vasko, B. D. Rekken, A. Mansikkamäki, J. C. Fettinger, H. M. Tuononen and P. P. Power, *Inorg. Chem.*, 2018, **57**, 6491–6502.

135 K. Nakamoto, in *Infrared and Raman Spectra of Inorganic and Coordination Compounds: Part B: Applications in Coordination, Organometallic, and Bioinorganic Chemistry*, John Wiley & Sons Inc., Haboken, New Jersey, 6th edn, 2009, pp. 314–316.

136 The central arene in plane C–C stretches were calculated to be 1433 cm^{-1}; a value that is in line with the observed increase of the M–arene interaction in complexes (**2-M**).

137 A. Logallo, L. C. H. Maddock, M. Mu, L. Gravogl, N. Jin, M. N. Peñas-Defrutos, K. Meyer, M. García-Melchor and E. Hevia, *Angew. Chem., Int. Ed.*, 2024, **63**, e202402907.

138 C. Y. Lin, J. C. Fettinger and P. P. Power, *Inorg. Chem.*, 2017, **56**, 9892–9902.

139 D. P. Halter, F. W. Heinemann, L. Maron and K. Meyer, *Nat. Chem.*, 2018, **10**, 259–267.

140 D. K. Modder, C. T. Palumbo, I. Douair, R. Scopelliti, L. Maron and M. Mazzanti, *Chem. Sci.*, 2021, **12**, 6153–6158.

141 M. Keener, R. A. K. Shivaraam, T. Rajeshkumar, M. Tricoire, R. Scopelliti, I. Zivkovic, A. S. Chauvin, L. Maron and M. Mazzanti, *J. Am. Chem. Soc.*, 2023, **145**, 16271–16283.